Temporal Lipid Profiling in the Progression from Acute to Chronic Heart Failure in Mice and Ischemic Human Hearts

Siddabasave Gowda B. Gowda, PhD[1,2], Divyavani Gowda PhD[1], Fengjue Hou[1], Hitoshi Chiba, MD, PhD[3], Vibhu Parcha, MD[4], Pankaj Arora, MD[4], Ganesh V. Halade PhD[5]*, Shu-Ping Hui, MD, PhD[1]*

1. Faculty of Health Sciences, Hokkaido University, Kita-12 Nishi-5, Kita-Ku, Sapporo 060-0812, Japan
2. Graduate School of Global Food Resources, Hokkaido University, Kita-12 Nishi-5, Kita-Ku, Sapporo 060-0812, Japan
3. Department of Nutrition, Sapporo University of Health Sciences, Nakanuma Nishi-4-3-1-15, Higashi-Ku, Sapporo 007-0894, Japan
4. Division of Cardiovascular Disease, Department of Medicine, University of Alabama at Birmingham, 35294
5. Division of Cardiovascular Sciences, Department of Medicine, University of South Florida, 560 Channelside Dr, Tampa, FL 33602, USA

Short title: Time-course of Lipid Species Profiling in Heart Failure

***Correspondence:**

1. Shu-Ping Hui

Faculty of Health Sciences, Hokkaido University, Kita-12 Nishi-5, Kita-Ku, Sapporo 060-0812, Japan ORCID: 0000-0001-9973-6461. e-mail address: keino@hs.hokudai.ac.jp

2. Ganesh V. Halade

Division of Cardiovascular Sciences, Department of Medicine, University of South Florida, Tampa, FL, USA ORCID: 0000-0002-5351-9354.

e-mail address: ghalade@usf.edu

Word count: 5350

Abstract:

Background and aims

Myocardial infarction (MI) is a leading cause of heart failure (HF). After MI, lipids undergo several phasic changes implicated in cardiac repair if inflammation resolves on time. However, if inflammation continues, that leads to end stage HF progression and development. Numerous studies have analyzed the traditional risk factors; however, temporal lipidomics data for human and animal models are limited. Thus, we aimed to obtain sequential lipidomics data from acute to chronic HF.

Methods

Here, we report the comprehensive lipidome of the hearts from diseased and healthy subjects. To induce heart failure in mice, we used non-reperfused model of coronary ligation and MI was confirmed by echocardiography and histology, then temporal kinetics of lipids in different tissue (heart, spleen, kidney), and plasma were quantitated from heart failure mice that compared with naïve controls. For lipid analysis in mice and human samples untargeted liquid chromatography-linear trap quadrupole orbitrap mass spectrometry (LC-LTQ-Orbitrap MS) was performed.

Results

In humans, multivariate analysis revealed distinct cardiac lipid profiles between healthy and ischemic subjects, with 16 lipid species significantly downregulated by 5-fold, mainly phosphatidylethanolamines (PE), in the ischemic heart. In contrast, PE levels were markedly increased in mouse tissues and plasma in chronic MI, indicating at possible cardiac remodeling. Further, fold change analysis revealed site-specific lipid biomarkers for acute and chronic HF. A significant decrease in sulfatides (SHexCer (34:1;2O)) and sphingomyelins (SM (d18:1/16:0)) was observed in mouse tissues and plasma in chronic HF.

Conclusions

Overall, a significant decreased lipidome in human ischemic LV and differential lipid metabolites in the transition of acute to chronic HF with inter-organ communication could provide a novel

insight in targeting integrative pathways for the early diagnosis or development of novel therapeutics to delay/prevent HF.

Keywords: Heart failure, Inflammation Biomarker, Multivariate analysis, Echocardiography, Histology, Lipidomics, Liquid chromatography/Mass spectrometry

Highlights

- A first integrative study using human and murine hearts on association of lipids in heart failure was investigated
- Lipid fingerprinting led to the identification of 273 species in clinical and mice samples
- A decrease in cardiac phosphatidylethanolamines is associated with human ischemic heart disease
- Inter-organ (heart, spleen, and kidney) and systemic lipid signatures were profiled in acute and chronic HF post-MI mice with decreased sulfatides (SHexCer (34:1;2O)) and sphingomyelins (SM (d18:1/16:0)) as plasma and tissue biomarkers of heart failure.

Graphical abstract:

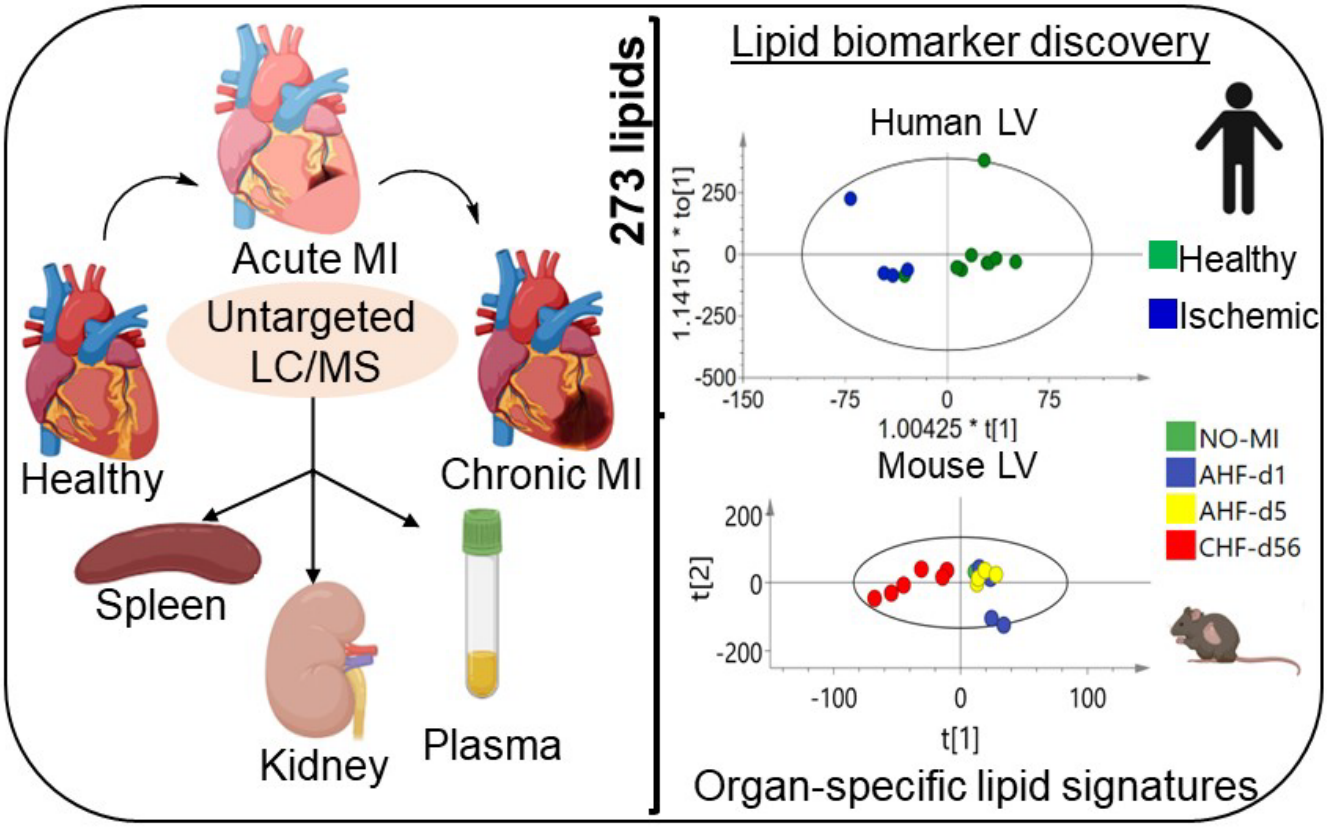

Abbreviations:

MI: myocardial infarction

HF: heart failure

AHF: acute heart failure

CHF: chronic heart failure

LV: left ventricle

PC: phosphatidylcholine

PE: phosphatidylethanolamine

PS: phosphatidylserine

PG: phosphatidylglycerol

PI: phosphatidylinositol

LPC: lysophosphatidylcholine

LPE: lysophosphatidylethanolamine

LPG: lysophosphatidylglycerol

LPI: lysophosphatidylinositol

SM: sphingomyelin

SM: Sphingomylein

Cer: ceramide

TAG: triacylglycerol

DAG: diacylglycerol

MAG: monoacylglycerol

CE: cholesterol ester

CL: cardiolipins

MLCL: mono-lysocardiolipins

HexCer: hexosylceramides

SHexCer: sulfatide

FFAs: Free fatty acids

CDP: Cytidine Diphosphate

1. Introduction

Cardiovascular diseases (CVD) are the major underlying cause of death worldwide, accounting for an estimated 17.8 million of all global deaths[1], and affecting over 37 million individuals worldwide[2]. Based on the NHANES 2015 to 2018 data, about 49.2% of adults (≥20 years) are at risk for CVD[3]. Epidemiological studies have established several risk factors for heart failure (HF)[4,5]. HF after myocardial infarction (MI) is a primary cause of late morbidity and mortality[6]. Advanced atherosclerosis leads to an MI event that results in irreversible damage to the myocardium due to a lack of oxygen, leading to impairment in systolic function. Since, both the incidence and prevalence of HF after post-MI have been increasing due to cardiometabolic defects such as obesity, LV diastolic dysfunction, diabetes, hypertension, and insulin resistance, it is essential to understand potential contributors to unresolved inflammation and HF[7]. At present, increased levels of plasma markers, such as creatinine kinase and cardiac troponin I, are used to determine the extent of myocardial injury[8]. However, more recent research interest has shifted toward identifying the temporospatial and prognostic biomarkers of HF progression in the early stages of cardiac injury and late cardiac remodeling[9].

In homeostasis, the heart is always in a state of high-energy demand for systole; the failing heart is incapable of supplying nutrients to different organs and to myocardium indication of heart dysfunction. Lipids, such as fatty acids are the largest contributors of energy (>70%) compared to other metabolic substrates. Among its potential cellular and molecular mechanisms, lipids are of central importance, because lipid mediators are directly linked to dietary patterns (nutrition), metabolic stress, and associated myocardial damage[10]. Cross-sectional investigations and experimental evidence support a link between serum lipid profiles and HF risk[11–13]. However, prospective human and temporal inter-organ mice studies that relate comprehensive lipidomics to the risk of developing HF are lacking. High-throughput quantitative

lipidomics using liquid chromatography/mass spectrometry (LC/MS) is a robust method for in-depth studies on lipid-related pathomechanisms. It also provides the possibility of developing new therapeutic targets for drugs discovery and development. Recent advances in mass spectrometry have allowed the application of technology to epidemiological cohorts of heart diseases in both human and animal studies[11,14–16].

This study was designed to profile lipids and obtain a progressive time-course from acute HF (AHF) to chronic HF (CHF), which are likely to be involved in HF using mouse samples. Also, we performed comprehensive lipidomic profiling in hearts from healthy controls and ischemic patients. Further, the association of 273 distinct lipid species with AHF and CHF was examined. The tissue and plasma lipid profiles were correlated with each other to identify possible lipid markers for HF.

2. Materials and Methods

2.1 Chemicals and Reagents.

High-purity LC/MS grade solvents, such as methanol, isopropanol, and a mobile-phase additive, 1M aqueous ammonium acetate, were obtained from Wako Pure Chemical Industries, Ltd. (Osaka, Japan). The ultrapure water used in this study was purified using a Milli-Q apparatus (Millipore, Bedford, USA). The extraction solvent chloroform (LC/MS grade) was purchased from Sigma-Aldrich (MO, USA). The deuterium-labeled internal standards for relative quantification of lipids, such as EQUIFLASH and oleic acid-d9, were supplied by Avanthi Polar Lipids (Alabaster, AL).

2.2 Human Samples and Animal Care Compliance

The human samples used in this study were approved by the Institutional Review Board of the University of Alabama at Birmingham. Heart tissue samples with active heart failure and control

were obtained from the biorepository (stored at -80 °C) of the University of Alabama at Birmingham. The healthy cardiac tissues were taken from individuals who had untimely death (accidental or gunshot) especially from left ventricle. The pathological ischemic heart disease samples were from the apex of myocardium area that was obtained during cardiac surgical procedure. The lipidomic analysis was approved by the ethical committee of Hokkaido University. Details regarding patient demographics and clinical signs are provided in supplementary information (**Table S1**). The mice were subjected to left anterior coronary ligation surgery (permanent ligation), and microsurgery was pre-approved by the Institutional Animal Care and Use Committees at the University of South Florida, Florida, USA. Further, all experimental protocols were according to the instructions of “Guide for the Care and Use of Laboratory Animals" (8th Edition. 2011) and the AVMA Guidelines for the Euthanasia of Animals (2013 Edition).

2.3 Experimental Design

The study design is presented in **Fig. 1A** and **1B** for the clinical and murine samples respectively. Mice were purchased from The Jackson Laboratory (#0006664) and kept under standard laboratory conditions (room temperature:19.8-22.2°C), with free access to water and a standard chow diet. Risk-free male mice (2-3 months old) were subjected to left anterior descending coronary ligation under continuous anesthesia (2-3% in compliance with the IACUC procedure). We precisely selected non-reperfused model over the ischemia-reperfusion model because of significant wall-thinning and definite systolic dysfunction due to coronary ligation[17]. For a temporal study of HF, mice were divided into three different groups: mice with no surgery as the naïve control (No-MI); mice with left anterior descending (LAD) ligation and sacrificed for organ harvest at day 1 and day 5, referred to as the AHF group (fractional shortening <10%); and mice with LAD monitored until day 56, referred to as the CHF group[17–19]. The plasma, infarcted LV, kidney, and spleen from post-MI and control samples were harvested for further lipidomic

analysis. We used exclusively infarcted left ventricle apex for MI samples, and left ventricle apex from control samples. The naïve control group was used as a control for the temporal changes in lipid species.

2.4 High-Resolution Echocardiography

For heart function measurement, the Vevo 3100 LAZR-X imaging system (Visual Sonics) equipped with a 40-MHz probe with a resolution of 30 μm. Echocardiographic images were acquired in the form of movie and then analyzed for various parameters of cardiac contractility and left ventricle wall dimensions, and volumes as described previously[20].

2.5 Histology

Spleen, kidney, and LV mid-cavity longitudinal sections were embedded in paraffin, sectioned and stained. Haematoxylin and eosin staining was employed for gross histological examination and validation of progressive wall-thinning suggestive of acute and chronic heart failure. Images were taken for each mouse (n=5-6/group) using a Keyence microscope (BZ X810) [18].

2.6 Extraction of lipids

For comprehensive lipid profiling, total lipids were extracted from the snap-frozen tissues and plasma using the method established in our laboratory with slight modifications [21,22]. A summary of the extraction workflow and mass spectrometry platform is shown in **Fig. 1C**. Concisely, 20-50 mg of snap-frozen mouse tissue (LV, spleen, and kidney) or 30 mg of Human LV were weighed into a 1.5-mL Eppendorf preloaded with 5–6 ceramic beads (1.4 mm, Cat. No. 15-340-159, Fisherbrand), and homogenized for 30 s (x 2 cycles) using a BeadMill 4 (Fisherbrand) homogenizer. Then, 10v of cold methanol was added, and the mixture was homogenized again for 30 sec (x 2cycles). Tissue homogenates (100 μL) were used for total lipid extraction. In the case of plasma samples, 50 μL was used directly. Then, about 100 μL of the homogenate was transferred to a new 1.5 mL tube, and 100 μL of the internal standard

mixture was mixed in methanol (having 10 ng of each of the following labelled standards: phosphatidylcholine (PC) (15:0-18:1(d7)), phosphatidylethanolamine (PE) (15:0-18:1(d7)), phosphatidylserine (PS) (15:0-18:1(d7)), phosphatidylglycerol (PG) (15:0-18:1(d7)), phosphatidylinositol (PI) (15:0-18:1(d7)), lysophosphatidylcholine (LPC) (18:1(d7)), lysophosphatidylethanolamine (LPE) (18:1(d7)), sphingomyelin (SM) (d18:1/18:0(d9)), ceramide (Cer) (d18:1/15:0 (d7)), triacylglycerol (TAG) (15:0-18:1(d7)-15:0), diacylglycerol (DAG) (15:0-18:1(d7)), cholesterol ester (CE) (18:1(d7)), monoacylglycerol (18:1(d7)), and 100 ng of oleic acid (d9). The mixture was vortexed at 3500 rpm for 30 s at room temperature. Subsequently, 400 µL of chloroform (vortex, 5 min, 3500 rpm) and 100 µL of Milli-Q (vortex, 30 s, 3500 rpm) were added. The biphasic extracts were centrifuged at 15000 rpm for 10 min at 4°C, the lower chloroform layer was transferred to a vial, and the upper layer was re-extracted with an additional 400 µL of chloroform. The chloroform extracts were combined and concentrated within a vacuum. The dried lipids were redissolved in 100 µL of methanol with gentle vortexing, centrifuged (15000 rpm, 10 min), and transferred to LC/MS vials. Extracts were injected into the LC/MS via an autosampler with each run set to an injection volume of 10 µL.

2.7 Lipidomic analysis by UHPLC/LTQ Orbitrap MS

Lipidomic analysis was performed using ultra-high-performance liquid chromatography with a linear ion trap quadrupole-Orbitrap mass spectrometry (UHPLC-LTQ Orbitrap MS) system consisting of an Orbitrap LTQ XL mass spectrometer (Thermo Fisher Scientific Inc., San Jose, CA) and LC-20AD HPLC (Shimadzu Corp., Kyoto, Japan). Separations were performed on an Atlantis T3 C18 column (2.1 × 150 mm, 3 µm, Waters, Milford, MA) with a mobile phase (A: aqueous 10 mM CH_3COONH_4, B: isopropanol, C: methanol) flow rate of 0.2 mL/min at 40 °C. In the negative mode analysis, a linear gradient of 0-1 min (30% B and 35% C), 1-14 min (80% B and 10% C), 14-27 min (85% B and 10% C), and 27-30 min (30% B and 35% C) were used. In the positive mode analysis, a linear gradient of 6% B and 90% C (0-1 min), 83% B and 15% C

(1-10 min), 83% B and 15% C (10-19 min), 6% B and 90% C (19-19.5 min), and 6% B and 90% C (19.5-22 min). MS analysis was carried out in both negative and positive electrospray ionization (ESI) in a Fourier transform mode with a resolving power of 60,0000 for the MS^1 mode at a collision energy of 35 V, capillary temperature (330 °C), nitrogen-sheath gas flow (50 units), and nitrogen-auxiliary gas (20 units). The MS conditions were identical to those reported in our previous report [21,22]. For the negative mode (scan range: *m/z* 150–1700), source and capillary voltages were set to 3 kV and 10 V, respectively, whereas for the positive mode (scan range: *m/z* 250–1600) it was 4 kV and 25 V respectively. Low-resolution MS/MS spectra were obtained at a collision energy of 40 V in the ion-trap mode. The obtained raw data were subjected to peak processing, alignment, and integration with a mass tolerance of 5.0 ppm using MS DIAL (version 4.2) and Xcalibur 2.2 software. The relative levels of lipids were calculated by taking the peak area ratios of the analyte to the internal standard and multiplying it by the amount of the added internal standard, following the guidelines of Lipidomics Standards Initiative level 2 and level 3 (https://lipidomics-standards-initiative.org/).

2.8 Statistical Analysis.

The results were plotted using Excel 2016 and GraphPad Prism version 8.0.1. Two-way ANOVA with Tukey multiple comparison test using GraphPad prism or Student's t-test using Excel 2016 was applied with $p<0.05$, which was considered to be statistically significant. Multivariate principal component analysis was performed using the online version of MetaboAnalyst 5.0 (https://www.metaboanalyst.ca) and ClustVis (https://biit.cs.ut.ee/clustvis/), according to the user instructions provided All data are presented as the mean ± standard error.

3. Results

3.1 Dysregulation of lipid metabolism in the human ischemic heart

To maintain homeostasis, the heart uses large amounts of fatty acids (>70%) as energy-providing substrates. The physiological balance between lipid uptake and oxidation prevents the accumulation of excess lipids. Despite the experimental and clinical data provide evidence that lipid accumulation causes or exacerbates heart dysfunction, limited reports have aimed to profile lipids in the heart tissue. Comprehensive lipid analysis of the human ischemic heart was performed, and the results are shown in **Fig. 2**. The volcanic plot ($p<0.05$) of all acquired lipid species in the LV is shown in **Fig. 2A**. Among the 273 annotated lipids, 16 lipid molecular species were significantly downregulated, and two lipids (LPC 19:0 ($p=0.005$), and SHexCer (34:1;3O) ($p=0.04$)) were upregulated by five folds in ischemic LV. Among the key downregulated lipids, seven molecular species were phosphatidylethanolamine (PEs), indicating that this class of lipids is a major biomarker of ischemia. Furthermore, the sphingolipid metabolite HexCer (d18:1/16:0), TAG 62:14, and fatty acids FA 22:2 and FA 20:4 were also significantly decreased in the LV of humans with ischemic heart disease by more than 10-fold.

The multivariate orthogonal projections of latent structures discriminant analysis (OPLSDA) and its S-plot of healthy vs. ischemic LV are shown in **Fig. 2B**. The data demonstrated a distinct separation between the healthy and ischemic groups. The variable of largely contributed lipid species for group separation is provided in the supplementary information (**Table. S2**). Furthermore, the significantly altered lipid classes of ischemic LV are shown in **Fig 2C**. In particular, phospholipids such as PC, PI, PS, PE, and lyso-PLs, including LPCs, LPGs, are significantly downregulated in ischemic LV. These results are consistent with a previous report that demonstrated a significant reduction in glycerophospholipid species in the infarcted LV of the ischemic human heart [23]. Energy-associated lipids, such as cardiolipins, and their lyso-cardiolipins are also downregulated following ischemic injury. Total hexosylceramides were also significantly decreased in ischemic LV. The lipid classes, including TAG, DAG, CE, SM, and PGs, also showed a decreasing trend despite insignificant statistical

differences. Other unaltered lipid classes are provided in the supplementary information (**Fig. S1**). The decreased TAG levels in the human ischemic heart were consistent with a previous study [23]. Thus, comparison of ischemic patients and healthy hearts using untargeted lipidomic analyses revealed a notable decrease in seven molecular species (TAG 62:14, HexCer (d18:1/16:0), FA 22:2, FA 20:4, PE (16:0/18:2), LPC 18:2, FA 22:1), and an increase in SHexcer (34:1;3O) as determined by mass spectrometry.

3.2 Validation of acute and chronic HF and multivariant analysis of the lipidome

Coronary ligation was successfully achieved that resulted in wall-thinning, high systolic and diastolic volume in mice, which was indicative of ischemic injury. We have collected infarcted left ventricle apex for MI samples, and left ventricle apex from control samples. The progression from AHF to CHF was monitored using high-resolution echocardiography (**Fig. 3A**). After MI, obvious heart dysfunction with marked dilation of the LV from day 1 onwards to day 56 is a severe form of heart failure. The speckle-tracking-based strain analysis of LV trace results showed immediate LV dysfunction on day 1 post-MI. The transition of AHF to CHF was marked by the sustained and irreversible progression of LV dysfunction, showing reduced fractional shortening on day 1, 5, and 56 post-MI (**Fig. 3A**). Histological changes in the LV were observed by severe myocardial apoptosis/necrosis of the infarcted area and posterior wall-thinning, indicative of CHF with an ejection fraction of 16±2% at day 56 post-MI. In the chronic phase of myocardial healing and repair from day 5 to day 56, sustained wall-thinning, systolic dysfunction, reduced cardiac output, and dilatation indicated CHF signs post-MI (**Table 1**). The fetal gene expression in the cardiac tissue that indicates cardiac damage, such as atrial natriuretic peptide (ANP) and brain natriuretic peptide (BNP) are provided in the supplementary information (**Fig. S2).**

Hematoxylin and eosin staining of the transverse LV mid-cavity from No-MI to days 1, 5, and 56 post-MI showed signs of progressive end-stage HF with wall-thinning, amplified necrosis in peri-infarct, and infarct area with LV remodeling and scar formation from MI day 5 onward to day 56 of CHF (**Fig. 3B**). The obvious structural changes in the heart were confirmed to be specific to myocardial necrosis by hematoxylin–eosin staining. Due to massive wall-thinning, the non-infarcted myocardium developed compensatory hypertrophy to meet the functional demand. Immediate splenic leukocyte depletion is a hallmark of ischemic injury, marked by spleen mass depletion in AHF. Kidney and splenic structural changes were also confirmed by hematoxylin and eosin staining (**Fig. 4A, B**). Permanent coronary ligation validates irreversible heart failure with marked heart dysfunction and structural wall-thinning in the infarcted region of the heart.

In total, 273 lipid molecular species from multiple lipid classes were identified in mouse tissues and plasma using untargeted LC/MS. The elution profiles are shown in **Fig. 4C**. Furthermore, each tissue and plasma-specific lipidome multivariate principal component analysis revealed a clear separation between the AHF and CHF groups (**Fig. 4D)**. However, limited separation was observed between the No-MI and AHF groups in both tissues and plasma. The ellipses indicate the clustering of the samples. The loading score plot represents the distribution of the most significant variables (i.e., lipids), along with the two first principal components and groupings between the samples. PC1 and PC2 accounted for 59.5% (LV), 60.4% (spleen), 67.7% (kidney), and 59.3% (plasma) of the model's total variance, and most of the variance was explained by PC1 31.6%, 35.5%, 41.1%, and 37.6%, respectively.

Large positive or negative loading scores indicate that a variable has a strong effect on that principal component. In the LV, lipids such as PE (O-16:1/18:2), PE (O-20:1/22:5), PE 36:5(O-16:1/20:4), PG (16:1/18:2), large positive loadings (loading score>0.1) and SM (d18:1/16:0) as the large negative loadings (loading score= -0.10) were seen along the PC1 axis. However, the PC2 axis showed strong negative loadings (-0.10) for 42 molecular species of TAGs. The spleen

showed mixed variance in the PC1 axis loadings, PEs such as PE (18:0/2:4), PE (O-20:1/22:5), PE (O-16:1/20:4), PE (16:0/22:6) as the large positive loadings (>0.09), and the LPE (O-16:1) and SM (d18:1/16:0) as large negative loadings (-0.09). However, the PC2 axis showed a strong positive loading (>0.10) for molecular species of TAGs. In the kidney, the PC1 axis has a large negative loading for lipids, such as Cer (d18:1/24:1), Cer (d18:1/24:0) (>-0.09) and PC2 axis as large positive loadings for lipids including TAG 43:4, monounsaturated fatty acids; FA 17:1, FA 21:1, FA 20:1. FA 18:1 and HexCer (d18:1/16:0) (>0.10), respectively. Finally, among the plasma lipidome, PE (O-16:1/18:2), PE (O-16:1/20:4), LPC 19:0, and LPC 16:1. LPE 20:4, PE (18:0/22:4, PE (18:0/20:3) had large positive loadings (>0.09) and SM (d18:1/16:0) as large negative loadings (-0.90) along the PC1 axis. Again, similar to the spleen, TAGs are predominant, with large positive loadings along the PC2 axis (>0.11), contributing majorly to the group separation in plasma. The separation of AHF and CHF mice groups in the PCA score plots of plasma and organs (LV, spleen, and kidney) lipidome data suggests a possible link between circulating lipid profiles and inter-organ connections in the physiology of mice with HF. In particular, lipidomic changes between No-MI to days 1 and 5 (AHF) are limited as shown by overlapping ellipses. However, day 56 (CHF) group showed a large variation compared to No-MI and AHF groups. Further, a major lipid changes were observed in the spleen and kidney tissues at MI Day 56 as demonstrated by the large variation in the score plots shown in Fig. 4D. Overall, these large variations in the PCA score plots between No-MI and CHF group of plasma and organs (LV, spleen, Kidney) indicates the inter-organ pathophysiology during HF.

3.3 Kinetics of lipidomic changes during AHF and CHF in mouse LV, spleen, kidney, and plasma

The heatmap representation of the cluster correlation analysis results is shown in **Fig. 5A.** The relative amounts of each type of lipid from acute (MI-day1, MI-day5) to chronic (CHF-day56) heart failure in the LV, spleen, kidney, and plasma are shown in **Fig. 5B**. The heatmap provides intuitive visualization of a lipid type, with each colored cell on the map corresponding to a relative concentration value of the lipids, with samples in rows and lipids in columns. It is used to identify samples in which lipids are high/low. Phosphatidylcholine (PC) is unchanged in tissues, whereas a significant increase was observed in plasma at CHF. In addition, the hydrolyzed product lyso-PC (LPC) was increased significantly in the plasma but decreased in the spleen and kidney under CHF conditions. Despite a slight decline in phosphatidylethanolamine (PE) in the LV at AHF (MI-day5), a significant rise was seen in CHF in the LV, spleen, kidney, and plasma. Contradictorily the hydrolyzed product lyso-PE (LPE) was increased only in plasma, whereas it decreased significantly in the LV, spleen, and kidney. Phosphoglycerol (PG) is decreased in the spleen, kidney, and plasma but its derivative lyso-phosphoglycerol (LPG) is elevated in spleen and plasma in CHF respectively. Additionally, lyso-phosphatidylinositol (LPI) is increased in the LV but decreases in the plasma at CHF. In contrast, lyso-phosphatidylserine (LPS) appeared to be significantly reduced in all tissues and plasma at the CHF.

Interestingly, the energy metabolism associated with lipids, such as cardiolipin (CL) and monolyso-cardolipin (MLCL), is significantly decreased in the plasma and LV of the CHF group. Furthermore, upregulation of fatty acid metabolism in the LV and cholesterol ester metabolism in the spleen were observed in the CHF groups when compared with controls. In our previous study, we demonstrated the significance of sphingoid bases and sphingosine-1-phosphate on cardiac repair mechanisms[19]. In particular, a decline in the levels of sphingolipid biosynthesis precursors, sphinganine, and sphingosine, was observed in the LV, spleen, and plasma in mice with chronic HF post-MI. In this study, the complex sphingolipids such as ceramides (Cer), hexosylceramides (Hexcer), sulfatides (SHexCer), and sphingomyelins (SM) were all

significantly downregulated in the tissues and plasma of CHF samples. However, a slight increase was seen in the ceramide levels in the LV during the acute phase. Despite the exception of some molecular species such as HexCer (d18:1/16:0), downregulation of sphingolipid metabolism was mostly observed during chronic HF. The hierarchical cluster correlation analysis showed a tight cluster between the plasma, LV, and spleen lipidomes. Furthermore, the decreased cardiolipins in the LV and increased lyso-PLs in plasma are demonstrated by the distinct variation in their color grades. The other lipids that were unchanged or not significant are provided in the supplementary information (**Fig. S1**). Although the results were not significant, an increase in plasma diacyl and triacylglycerols was observed.

To identify the group (acute and chronic) specific lipid molecular species, logarithmic fold change analysis was performed between No-MI vs. AHF-day1, No-MI vs. AHF-day5, and No-MI vs. CHF-day 56 in the LV, spleen, kidney, and plasma, respectively. The results are provided in the Supplementary Information (**Table S3-S6**). The key lipid pathways/lipid molecular species altered in acute MI are; PG upregulation and PE downregulation in the LV, LPE 20:5, PG (20:5/22:5) downregulation in the spleen, TAG upregulation in the kidney, and increased SHexCer levels or decreased LPIs (LPI 20:4, LPI 18:2, LPI 20:3) in plasma. In chronic MI, downregulation of SHexCer and SM are common in the LV, spleen, and kidney, but SHexCer (34:1;3O) is upregulated in human LV. Further, upregulation of CEs in the spleen, FA 22:1, HexCer (d18:1/16:0) in the LV, FA 20:4, and FA 22:2 in the kidney and TAGs in plasma were observed. These results suggest integrative pathophysiology of different organs and widespread impact of lipid species following cardiac injury in transition of acute to chronic heart failure.

3. Discussion

Ischemic heart disease is the major underlying cause of acute HF [24]. Accumulating evidence suggests that the underlying mechanisms responsible for HF include chronic inflammation,

oxidative stress, intracellular calcium overload, mitochondrial dysfunction, and abnormal lipid metabolism [25–28]. Previously, ^{1}H-NMR-based lipid profiling were carried out to detect the presence of ischemic heart disease[29]. Lipotoxicity due to cardiometabolic defects or intracellular lipid accumulation in plaque is one of the causes of ischemic event; however, there have only been a limited number of temporal lipidomic studies are conducted. Moreover, there is no integrative data on the lipid levels that interconnect plasma, spleen, kidney, and heart levels in cardiac repair from acute to chronic HF. In this study, we used an unbiased and untargeted LC/MS approach to profile lipids in patients with ischemic heart and tissue from post-MI mice. Due to biological and individual variation (age, sex, ethnicity, co-medication (s), time after ischemic event etc.) of human samples, we used mice for time-dependent kinetics of infarcted samples and different organs after cardiac injury and then compared with control heart and different organs from non-failing mice.

LC/MS is a highly sensitive and specific technique for lipid analysis and has been widely applied in cardiac biology for biomarker discovery[11,12,14,19]. Our key findings are as follows: 1) reduced glycerophospholipids especially PE, in patients with ischemic heart disease; conversely, 2) cardiac repair in risk-free mice was promoted by the rise of PEs in the LV, spleen, kidney, and plasma in CHF (MI day 56); 3). Downregulation of sphingolipid metabolism was associated with CHF except for the significant rise of HexCer (d18:1/16:0) through AHF to CHF. In the presented lipidomic analysis of both clinical and murine samples, 273 lipids were identified from five main lipid classes including 84 glycerolipids, 120 glycerophospholipids (GPL), 46 sphingolipids (SL), 17 fatty acyls, and 6 sterols. To date, there have been few lipidomic studies on murine ventricles but limited on human LV, due to the challenges of tissue harvest timing after ischemic events and region-specific myocardium samples. A recent study has shown the lipidomic analysis of human LV and infarcted LV. However, this is limited by the comprehensive profiling of lipid diversity. The results of human LV analysis in this study showed significant

downregulation of GPLs in ischemic patients. The levels of main GPLs, such as PC, PI, PS, PE, lyso-forms (LPC, LPG), and their complex energy-associated cardiolipins (CL and MLCL), are significantly decreased in patients with ischemic LV compared to control LV. These results are consistent with a previous clinical study that demonstrated decreased GPLs (PC, PE, PG) in infarcted LV[23] as well as in the LV of murine MI models [30]. These findings strongly support the GPL decay caused by ischemia-induced phospholipolysis of cardiomyocyte membranes with the up-regulatory effect of hypoxia on phospholipase activity [31].

Downregulation of CL and MLCL could have a serious impact on mitochondrial morphology, physiology, and function. These lipids are involved in controlling mitochondrial structure, respiratory activity, and oxidative stress [32,33]. Indeed, a significant loss of CL (for example, CL 74:8 by 6-folds) and MLCL might contribute to a serious decrease in mitochondrial oxidative metabolism in ischemic LV. A previous report is consistent with our results demonstrating decreased cardiac CL in patients with heart failure [34]. In the volcanic plot, the top 16 lipids that significantly decreased by more than 5-folds in ischemic LV, among them, PEs are mainly predominant. PEs are essential for heart function as they comprise the inner mitochondrial membrane [35], and their deficiency is associated with a dysfunction of autophagy and the formation of reactive oxygen species [36]. Studies in Drosophila suggest that inhibition of the synthesis of PE, causes cardiac dysfunction associated with elevated cardiac TAG levels [37]. Our results demonstrated a significantly decreased HexCer(d18:1/16:0) by 20-folds) and total HexCer in human ischemic LV, which contradicts previous results, noting an over time in infarcted LV [38]. However, increased SHexCer (34:1;3O) levels may be consistent with a previous in vivo report that demonstrated an upregulation of SHexCer in post-MI [39]. Despite a positive correlation between fatty acids such as arachidonic acid and the risk of ischemic heart disease[40] in our study FA 20:4 and FA 22:2 levels were significantly reduced by 10-fold in ischemic LV suggesting dysregulation of these specific fatty acids. In comparison to current

reports, this is the first comprehensive report on the analysis of fatty acids in human LVs. Glycerolipids (DAG, TAG) and sterol (CE) levels despite non-significant levels showed a decreasing trend in ischemic LV. Unsaturated TAGs were found to be decreased (TAG 62:14) in infarcted LV [38] and were found to be associated with reduced HF risk (TAG 58:7) [41]. Interestingly, our results also showed a significant reduction of TAG (62:14) by 27-fold in ischemic human LV, suggesting the significance of the balance of unsaturated TAGs in HF risk.

Furthermore, to understand the time-dependent physiological changes in lipid profiles in acute and chronic MI, an MI model using risk-free mice was used and the inter-organ lipid signatures were obtained. The present results integrate LV, spleen, kidney, and plasma lipidomes in murine AHF and CHF pathophysiology. The summary of the lipidomic changes in both human ischemic heart and mouse MI is represented in a pathway as described in **Fig. 6**. The results demonstrated the dysregulation of GPLs (PC, PE, PG, CL, MLCL, LPC, and LPE) and SL metabolism in both tissues and plasma. In the LV, the decreased levels of PE in acute MI (Fig. 5B) are consistent with human ischemic LV. However, in the chronic stage, PE levels return to normal, which is possible due to the activation of cardiac repair mechanisms via inter-organ coordination in the absence of risk factor(s) in mice (young mice versus aging ischemic patients). A profound increase in PE levels was observed in CHF in the spleen, kidney, and plasma. Despite the total PCs being unchanged in tissues a significant increase in plasma was detected in CHF. The enrichment of lipid PC (16:0/16:0) has been reported to be a plasma lipid biomarker with a higher HF risk[25]. In our results, plasma PC (16:0/16:0) was increased by 2-fold in the CHF group compared to that in the No-MI group.

PG plays a pivotal role in the formation of cardiolipin, which is essential for mitochondrial structure, and function. In this study, a significant decline in PG levels was observed in the spleen, kidney, and plasma, but not in the mouse LV in CHF. Downregulated PG levels were

reported earlier in human infarcted LV [38]; however, resistance to such changes in mouse LV could be attributed to cardiac repair mechanisms. Moreover, functional cardiolipin downregulation was observed in the LV and plasma, and expected mechanisms were similar to those proposed for human data. The free fatty acids in the LV and cholesterol esters in the spleen are notably increased at CHF. Elevated plasma free fatty acids are positively associated with the development of MI and deleterious effects on heart function[42]. Cholesterol esters accumulate in the heart in a porcine model of ischemia [43]; however, but in our results, despite a slight increase in AHF, significant accumulation was seen in the spleen in CHF suggest integrative changes in lipid metabolism.

The significant downregulation of sphingolipids (SL), such as total ceramides, hexosylceramides, and sphingomyelin at CHF in mice plasma and organs suggests possible cardiac remodeling. The abnormal accumulation of ceramides has been implicated in acute MI and myocardial failing [44,45]. Interestingly, SL metabolite, sulfatides (SHexCer) are accumulated in acute LV. However, a significant decline in their levels is observed in chronic LV. Sulfatides have been reported to be associated with a heritable cardiac risk and positively correlated with total cholesterol[46]. In an ST-segment elevation MI study high levels of circulating sulfatides were found to be positively correlated with an increased rates of hospital death and complications [47]. In this study of human LV, we found an increase in sulfatides in ischemic LV, although without any statistical significance (Fig. S1). In other words, a major decrease of sulfatides in CHF was observed in mice, suggesting possible cardiac remodeling.

We demonstrated region-specific lipid biomarkers at the molecular species level by adding them to the main lipid class changes. Among the top altered species, HexCer (d18:1/16:0) and PG (20:5/22:5) increased, while LPG 16:0 and SHexCer (40:2;2O) were decreased in the LV at AHF. In addition, HexCer (d18:1/16:0) and SM (d18:1/16:0) were the largely up-and down-regulated

species at CHF, respectively. Similarly, SHexCer (41:1;2O) and HexCer (d18:1/16:0) were significantly increased, and LPI 20:3 and CL76:12 were decreased in plasma of mice at AHF. Chronic HF plasma biomarkers are TAG 62:3 (upregulated) and SM (d18:1/16:0) (downregulated). An immunoregulatory organ such as the spleen also showed large lipidomic changes in CHF rather than AHF in mice, suggesting inter-organ lipid signaling in the spleen for cardiac repair mechanisms. The key splenic up and downregulated biomarkers were CE 22:4 and SM (d18:1/16:0), respectively, at CHF.

In AHF, impaired renal function was commonly observed[48], thus, it is important to understand lipid networks of the heart and kidney in AHF. In the kidney, our data showed a large number of upregulated unsaturated TAGs as markers of AHF. FA 20:4 and SHexcer (34:1;2O) were largely up-and down-regulated lipid species in CHF in mice. Past studies are limited to lipidomic analyses of either circulating or cardiac lipids in HF. Of note, this is the first comprehensive report of human ischemic heart lipid profiling and mouse samples with lipid fingerprinting through acute to chronic AHF.

The main limitations of this study are the low number of patient samples and lack of precise information on the myocardium regions and time of harvest after the ischemic event, thus termed as LV samples. We had limited access to functional and morphometry data from healthy patients because the myocardium tissue harvested during cardiac surgery. Critically, we have selected consistent myocardium samples for analyses therefore, we have limited samples. The human LV control specimens were from autopsied victims of accidents and are compared with samples obtained from patients with ischemic heart disease, which could have some impact on lipid data. The storage time of the cadavers may have affected the lipid composition of the heart. Thus, there is indeed a risk that the lipid composition of the control human samples may have changed before the autopsy. Control and ischemic samples had relatively different time of harvest due to

heterogeneous nature of clinical setting. Of note, clinical samples data used for proof-of-concept and real-time dependent kinetics supported by pre-clinical studies outcome. Second, the lipid analysis results were semi-quantitative. Co-medication has a critical impact on lipid profiling (e.g., NSAIDs and doxorubicin), which is not considered in this limited patient sample set [20,49] and the effect of anaesthesia, stress, and other factors that influence lipidomic changes associated with myocardial ligation are not considered. Further post-mortem samples could have some impact on lipidomic changes as demonstrated in previous studies[50,51]. In the presented case, the temporal lipid profiling performed using young male risk-free mice (healthy), however use of aging-related and sex-specific differences are expected in lipid species that warrant further investigation.

In conclusion, we identified specific lipid metabolites and inter-organ lipidomic patterns that were significantly associated with HF in mice with acute to chronic MI and human ischemic heart samples. The word “inter-organ” was used to indicate integrative and comprehensive changes in total body to indicate health possible reflection in plasma. The untargeted LC/MS analysis revealed strong lipid remodeling that resulted in significantly reduced levels of PE, PC, PI, PS, LPC, LPG, CL, MLCL, and HexCer in ischemic human LV (pathological lipid remodelling). To explore the lipid biomarkers of acute and chronic HF and inter-organ coordination in cardiac remodeling, the kinetic lipidomic profile in mice was assessed using echocardiography, histology, and LC/MS analysis. A decrease in mitochondrial function associated with lipids, such as PE, PG, and CLs, appeared to be an early marker of AHF. However, increased PEs at CHF suggest possible cardiac remodeling in mice (physiological lipid remodelling). As for clinical implication, plasma is the only sample easily accessed and lipidomics can be performed. Our results suggest that lipid fingerprinting may provide advanced tools for HF biomarker prognosis and progression; thus, targeting lipid signaling in molecular and cellular pathways provides the foundation for the discovery of new therapeutics.

Supplemental data

Supplemental Tables S1-S6 and Figure S1, S2.

Acknowledgements:

We acknowledge the support in part from National Institutes of Health [grant HL144788 and HL132989] to GVH. Japanese Society for the Promotion of Science (JSPS) KAKENHI [grants 18K0743408, 19H0311719, and 19K0786109] to S-P Hui. Faculty of Health Sciences for the research support [grant 870411Q] and JSPS early carrier scientist [grant 21K1481201] to SGBG. We would like to thank Editage (www.editage.com) for English language editing and Graduate School of Global Food Resources, Hokkaido University for the financial aid.

Conflict of interest

The authors declare no conflicts of interest associated to the study.

Data availability statement

The data are available upon request to first or corresponding authors.

Author contributions

S.G.B.G. and G.V.H. conceived and designed research; S.G.B.G., D.G., F.H., H.C. S.-P.H., and G.V.H. performed experiments; S.G.B.G., D.G., F.H., H.C., S.-P.H., V.P., P.A., and G.V.H. analyzed data; S.G.B.G., D.G., F.H., V.P., P.A., and G.V.H. interpreted results of experiments; S.G.B.G., D.G., S.-P.H., and G.V.H. prepared figures and drafted manuscript; S.-P.H. and G.V.H. edited and revised manuscript; S.G.B.G., D.G., F.H., H.C., S.-P.H., V.P., P.A., and G.V.H. approved final version of manuscript.

References

[1] V. SS, A. A, B. EJ, B. MS, C. CW, C. AP, C. AM, C. AR, C. S, D. FN, D. L, E. MSV, F. JF, F. M, K. SS, K. BM, K. KL, K. TW, L. DT, L. TT, L. JH, L. CT, L. MS, L. PL, M. SS, M. K, M. AE, M. ME, P. AM, R. WD, R. GA, S. UKA, S. GM, S. EB, S. SH, S. CM, S. NL, S. A, T. DL, V. LB, T. CW, Heart Disease and Stroke Statistics-2020 Update: A Report

From the American Heart Association, Circulation. 141 (2020) E139–E596. https://doi.org/10.1161/CIR.0000000000000757.

[2] G. Savarese, L.H. Lund, Global Public Health Burden of Heart Failure, Card Fail Rev. 3 (2017) 7. https://doi.org/10.15420/CFR.2016:25:2.

[3] V. SS, A. A, A. HJ, B. EJ, B. MS, C. CW, C. AP, C. AM, C. S, D. FN, E. MSV, E. KR, F. JF, G. DK, K. SS, K. BM, K. KL, L. CD, L. TT, L. J, L. MS, L. PL, M. J, M. J, M. SS, M. DB, M. ME, N. SD, P. AM, R. GA, S. Z, S. GM, S. EB, S. SH, S. CM, S. A, V. LB, W. NY, T. CW, Heart Disease and Stroke Statistics-2021 Update: A Report From the American Heart Association, Circulation. 143 (2021) E254–E743. https://doi.org/10.1161/CIR.0000000000000950.

[4] G.A. Gaesser, S.S. Angadi, Obesity treatment: Weight loss versus increasing fitness and physical activity for reducing health risks, IScience. 24 (2021) 102995. https://doi.org/10.1016/J.ISCI.2021.102995.

[5] S. BW, O. AJ, C. KL, R. CM, Risk Prediction Models for Incident Heart Failure: A Systematic Review of Methodology and Model Performance, J Card Fail. 23 (2017) 680–687. https://doi.org/10.1016/J.CARDFAIL.2017.03.005.

[6] J. D, M. V, S. J, S. V, K. J, K. J, A. V, W. P, Heart failure after myocardial infarction: incidence and predictors, ESC Heart Fail. 8 (2021) 222–237. https://doi.org/10.1002/EHF2.13144.

[7] G. V. Halade, V. Kain, Obesity and Cardiometabolic Defects in Heart Failure Pathology, Compr Physiol. 7 (2017) 1463–1477. https://doi.org/10.1002/CPHY.C170011.

[8] Y. Wu, N. Pan, Y. An, M. Xu, L. Tan, L. Zhang, Diagnostic and Prognostic Biomarkers for Myocardial Infarction, Front Cardiovasc Med. 7 (2020) 617277. https://doi.org/10.3389/FCVM.2020.617277.

[9] S.-R. A, P.-E. M, M. M, S. D, R. S, S. T, Novel Biomarkers of Heart Failure, Adv Clin Chem. 79 (2017) 93–152. https://doi.org/10.1016/BS.ACC.2016.09.002.

[10] G. IJ, T. CM, S. PC, Lipid metabolism and toxicity in the heart, Cell Metab. 15 (2012) 805–812. https://doi.org/10.1016/J.CMET.2012.04.006.

[11] D. D, P. R, R. D, H. T, H. M, Serum untargeted lipidomic profiling reveals dysfunction of phospholipid metabolism in subclinical coronary artery disease, Vasc Health Risk Manag. 15 (2019) 123–135. https://doi.org/10.2147/VHRM.S202344.

[12] H. GV, K. V, T. B, J. JK, Lipoxygenase drives lipidomic and metabolic reprogramming in ischemic heart failure, Metabolism. 96 (2019) 22–32. https://doi.org/10.1016/J.METABOL.2019.04.011.

[13] L. Yang, L. Wang, Y. Deng, L. Sun, B. Lou, Z. Yuan, Y. Wu, B. Zhou, J. Liu, J. She, Serum lipids profiling perturbances in patients with ischemic heart disease and ischemic cardiomyopathy, Lipids Health Dis. 19 (2020). https://doi.org/10.1186/S12944-020-01269-9.

[14] L. Yang, L. Wang, Y. Deng, L. Sun, B. Lou, Z. Yuan, Y. Wu, B. Zhou, J. Liu, J. She, Serum lipids profiling perturbances in patients with ischemic heart disease and ischemic cardiomyopathy, Lipids Health Dis. 19 (2020). https://doi.org/10.1186/S12944-020-01269-9.

[15] M. Barchuk, A. Dutour, P. Ancel, L. Svilar, V. Miksztowicz, G. Lopez, M. Rubio, L. Schreier, J.P. Nogueira, R. Valéro, S. Béliard, J.C. Martin, G. Berg, B. Gaborit, Untargeted Lipidomics Reveals a Specific Enrichment in Plasmalogens in Epicardial Adipose Tissue and a Specific Signature in Coronary Artery Disease, Arterioscler Thromb Vasc Biol. 40 (2020) 986–1000. https://doi.org/10.1161/ATVBAHA.120.313955.

[16] M.L. Cheng, C.H. Wang, M.S. Shiao, M.H. Liu, Y.Y. Huang, C.Y. Huang, C.T. Mao, J.F. Lin, H.Y. Ho, N.I. Yang, Metabolic disturbances identified in plasma are associated with outcomes in patients with heart failure: diagnostic and prognostic value of metabolomics, J Am Coll Cardiol. 65 (2015) 1509–1520. https://doi.org/10.1016/J.JACC.2015.02.018.

[17] L. ML, B. KR, K. JA, K. P, C. JW, de C.B. LE, D.-P. KY, D.R. DP, F. NG, F. S, G. RJ, H. G, J. SP, R. RH, S. FG, T. EB, R. CM, K. Z, Guidelines for in vivo mouse models of myocardial infarction, Am J Physiol Heart Circ Physiol. (2021). https://doi.org/10.1152/AJPHEART.00459.2021.

[18] G. v. Halade, V. Kain, K.A. Ingle, Heart functional and structural compendium of cardiosplenic and cardiorenal networks in acute and chronic heart failure pathology, Am J Physiol Heart Circ Physiol. 314 (2018) H255–H267. https://doi.org/10.1152/ajpheart.00528.2017.

[19] B.G. S, G. D, K. V, C. H, H. SP, C. CE, P. V, A. P, H. GV, Sphingosine-1-phosphate interactions in the spleen and heart reflect extent of cardiac repair in mice and failing human hearts, Am J Physiol Heart Circ Physiol. 321 (2021) H599–H611. https://doi.org/10.1152/AJPHEART.00314.2021.

[20] H. GV, K. V, W. GM, J. JK, Subacute treatment of carprofen facilitate splenocardiac resolution deficit in cardiac injury, J Leukoc Biol. 104 (2018) 1173–1186. https://doi.org/10.1002/JLB.3A0618-223R.

[21] S.G.B. Gowda, Z.-J. Gao, Z. Chen, T. Abe, S. Hori, S. Fukiya, S. Ishizuka, A. Yokota, H. Chiba, S.-P. Hui, Untargeted lipidomic analysis of plasma from high fat diet-induced obese rats using UHPLC- linear trap quadrupole -Orbitrap MS, Analytical Sciences. (2020) 1–20. https://doi.org/10.2116/analsci.19p442.

[22] S.G.B. Gowda, Y. Sasaki, E. Hasegawa, H. Chiba, S.P. Hui, Lipid fingerprinting of yellow mealworm Tenebrio molitor by untargeted liquid chromatography-mass spectrometry , J Insects Food Feed. 8 (2022) 157–168. https://doi.org/10.3920/JIFF2020.0119/ASSET/IMAGES/SMALL/GA_JIFF2020.0119.GIF.

[23] S. V, M. de L.S. IM, A. AB, V. D, D. J, C. J, J. E, C. DG, G. A, L. E, R. JMG, C. F, L. R, L.C. V, Biophysical and Lipidomic Biomarkers of Cardiac Remodeling Post-Myocardial Infarction in Humans, Biomolecules. 10 (2020) 1–20. https://doi.org/10.3390/BIOM10111471.

[24] A. M, J. M, M. W, R. N, S. AM, S. K, M. A, Acute heart failure, Nat Rev Dis Primers. 6 (2020). https://doi.org/10.1038/S41572-020-0151-7.

[25] W. C, E. F, T. E, G.-F. M, R.-C. M, L. J, A. F, L. CH, L. L, S.-S. J, C. CB, S. MB, M.-G. MÁ, H. FB, Lipid Profiles and Heart Failure Risk: Results From Two Prospective Studies, Circ Res. 128 (2021) 309–320. https://doi.org/10.1161/CIRCRESAHA.120.317883.

[26] G. PA, C. DK, H. RJ, Altered myocardial calcium cycling and energetics in heart failure--a rational approach for disease treatment, Cell Metab. 21 (2015) 183–194. https://doi.org/10.1016/J.CMET.2015.01.005.

[27] P. JN, S. A, G. N, P. TT, K. JQ, Mitochondrial dysfunction and oxidative stress in heart disease, Exp Mol Med. 51 (2019). https://doi.org/10.1038/S12276-019-0355-7.

[28] Z. Li, H. Zhao, J. Wang, Metabolism and Chronic Inflammation: The Links Between Chronic Heart Failure and Comorbidities, Front Cardiovasc Med. 8 (2021). https://doi.org/10.3389/FCVM.2021.650278.

[29] I. Kastani, C. Kostara, J. Baltogiannis, V. Tsimihodimos, M. Elisaf, J. Goudevenos, E. Bairaktari, Investigation of the presence of ischemic heart disease by the 1H NMR-based lipidomics of red blood cell membranes, Atherosclerosis. 241 (2015) e124–e125. https://doi.org/10.1016/j.atherosclerosis.2015.04.432.

[30] T. AT, Using metabolomics to assess myocardial metabolism and energetics in heart failure, J Mol Cell Cardiol. 55 (2013) 12–18. https://doi.org/10.1016/J.YJMCC.2012.08.025.

[31] Activation of a membrane-associated phospholipase A2 during rabbit myocardial ischemia which is highly selective for plasmalogen substrate - PubMed, (n.d.). https://pubmed.ncbi.nlm.nih.gov/2005103/ (accessed October 27, 2021).

[32] C. WW, C. YJ, C. WH, C. JF, H. YH, Phosphatidylglycerol Incorporates into Cardiolipin to Improve Mitochondrial Activity and Inhibits Inflammation, Sci Rep. 8 (2018). https://doi.org/10.1038/S41598-018-23190-Z.

[33] L. Pokorná, P. Čermáková, A. Horváth, M.G. Baile, S.M. Claypool, P. Griač, J. Malínský, M. Balážová, Specific degradation of phosphatidylglycerol is necessary for proper mitochondrial morphology and function, Biochimica et Biophysica Acta (BBA) - Bioenergetics. 1857 (2016) 34–45. https://doi.org/10.1016/J.BBABIO.2015.10.004.

[34] E. Smeir, S. Leberer, A. Blumrich, G. Vogler, A. Vasiliades, S. Dresen, C. Jaeger, Y. Gloaguen, C. Klose, D. Beule, P.C. Schulze, R. Bodmer, A. Foryst-Ludwig, U. Kintscher, Depletion of cardiac cardiolipin synthase alters systolic and diastolic function, IScience. (2021). https://doi.org/10.1016/j.isci.2021.103314.

[35] D. G, Lipids of mitochondria, Biochim Biophys Acta. 822 (1985) 1–42. https://doi.org/10.1016/0304-4157(85)90002-4.

[36] R. P, K. M, P. F, M. N, K. O, S. V, F. J, C.-G. D, K. G, M. F, Phosphatidylethanolamine positively regulates autophagy and longevity, Cell Death Differ. 22 (2015) 499–508. https://doi.org/10.1038/CDD.2014.219.

[37] L. HY, W. W, W. RJ, O. K, B. R, Phospholipid homeostasis regulates lipid metabolism and cardiac function through SREBP signaling in Drosophila, Genes Dev. 25 (2011) 189–200. https://doi.org/10.1101/GAD.1992411.

[38] S. V, M. de L.S. IM, A. AB, V. D, D. J, C. J, J. E, C. DG, G. A, L. E, R. JMG, C. F, L. R, L.C. V, Biophysical and Lipidomic Biomarkers of Cardiac Remodeling Post-Myocardial Infarction in Humans, Biomolecules. 10 (2020) 1–20. https://doi.org/10.3390/BIOM10111471.

[39] T. Hua, Q. Bao, X. He, W. Cai, J. He, Lipidomics Revealed Alteration of Sphingolipid Metabolism During the Reparative Phase After Myocardial Infarction Injury, Front Physiol. 12 (2021) 663480. https://doi.org/10.3389/FPHYS.2021.663480.

[40] H. LE, N. A, Arachidonic acid and ischemic heart disease, J Nutr. 135 (2005) 2271–2273. https://doi.org/10.1093/JN/135.9.2271.

[41] W. C, E. F, T. E, G.-F. M, R.-C. M, L. J, A. F, L. CH, L. L, S.-S. J, C. CB, S. MB, M.-G. MÁ, H. FB, Lipid Profiles and Heart Failure Risk: Results From Two Prospective Studies, Circ Res. 128 (2021) 309–320. https://doi.org/10.1161/CIRCRESAHA.120.317883.

[42] K. VA, O. MF, Free fatty acids during acute myocardial infarction, Prog Cardiovasc Dis. 13 (1971) 361–373. https://doi.org/10.1016/S0033-0620(71)80012-9.

[43] C. Drevinge, L.O. Karlsson, M. Ståhlman, T. Larsson, J.P. Sundelin, L. Grip, L. Andersson, J. Borén, M.C. Levin, Cholesteryl Esters Accumulate in the Heart in a Porcine Model of Ischemia and Reperfusion, PLoS One. 8 (2013) e61942. https://doi.org/10.1371/JOURNAL.PONE.0061942.

[44] H. Y, V. AS, Y. E, Ż. MM, C. E, S. N, S. MTK, G. N, K. R, K. AA, K. K, M. A, F. A, K. MG, H. N, K. E, D. NC, S. E, H. R, E. E, Z. L, Altering Sphingolipid Metabolism Attenuates Cell Death and Inflammatory Response After Myocardial Infarction, Circulation. 141 (2020) 916–930. https://doi.org/10.1161/CIRCULATIONAHA.119.041882.

[45] J. R, A. H, D. K, L. X, J. H, K. PJ, B. DL, C. E, Z. X, D. LY, H. S, G. IJ, T. H, N. Y, G. IJ, S. PC, Increased de novo ceramide synthesis and accumulation in failing myocardium, JCI Insight. 2 (2017). https://doi.org/10.1172/JCI.INSIGHT.82922.

[46] K. A, J. M, C. LA, Sphingolipids in the Heart: From Cradle to Grave, Front Endocrinol (Lausanne). 11 (2020). https://doi.org/10.3389/FENDO.2020.00652.

[47] G. Li, R. Hu, Y. Guo, L. He, Q. Zuo, Y. Wang, Circulating Sulfatide, A Novel Biomarker for ST-Segment Elevation Myocardial Infarction, J Atheroscler Thromb. 26 (2019) 84. https://doi.org/10.5551/JAT.43976.

[48] Impaired renal function in acute myocardial infarction - PubMed, (n.d.). https://pubmed.ncbi.nlm.nih.gov/19753517/ (accessed October 27, 2021).

[49] J. JK, W. GW, K. V, S. MA, S. R, Y. N, H. GV, Doxorubicin triggers splenic contraction and irreversible dysregulation of COX and LOX that alters the inflammation-resolution program in the myocardium, Am J Physiol Heart Circ Physiol. 315 (2018) H1091–H1100. https://doi.org/10.1152/AJPHEART.00290.2018.

[50] A.P. Hart, R.E. Zumwalt, A. Dasgupta, Postmortem lipid levels for the analysis of risk factors of sudden death: usefulness of the Ektachem and Monarch analyzers, Am J Forensic Med Pathol. 18 (1997) 354–359. https://doi.org/10.1097/00000433-199712000-00008.

[51] S. Ylä-Herttuala, T. Nikkari, Effect of post-mortem time on the biochemical composition of coronary arteries, Atherosclerosis. 56 (1985) 1–10. https://doi.org/10.1016/0021-9150(85)90079-6.

Table 1: Cardiac functional measurement of C57BL/6 mice in acute (AHF) and chronic heart failure (CHF) following myocardial infarction.

Groups /Echocardiography parameters	Naïve controls	MI-day 1 (AHF)	MI-day 5 (AHF)	MI-day 56 (CHF)
	Male (n= 8)	Male (n= 8)	Male (n= 9)	Male (n= 7)
Heart rate (bpm)	537 ± 19	489 ± 15	524 ± 23	489 ± 20
EDV (μl)	61 ± 2	91 ± 6¥	93 ± 11¥	130 + 20¥
ESV (μl)	22 ± 2	73 ± 7¥	74 ± 10¥	108 + 28¥
Ejection fraction	64 ± 2	27 ± 3¥	29 ± 3¥	16 + 2¥
Cardiac output (ml/min)	21 ± 1	8 ± 1¥	10 ± 2¥	12 + 8¥
IVSd (mm)	0.70 ± 0.04	0.56 ± 0.03¥	0.67 ± 0.05¥	0.22 + 0.03¥
PWTd (mm)	0.74 ± 0.03	0.70 ± 0.03¥	0.63 ± 0.04¥	0.32 + 0.02¥
IVSs (mm)	0.99 ± 0.07	0.66 ± 0.04¥	0.74 ± 0.06¥	0.34 + 0.04¥
PWTs (mm)	0.95 ± 0.04	0.78 ± 0.04¥	0.70 ± 0.04¥	0.35 + 0.05¥
Cardiac output (ml/min)	20.09 ± 2.16	4.79 ± 0.34	5.12 ± 0.66	4.93 ± 0.56
GCS	-16 ± 1	-10 ± 1¥	-11 ± 2¥	-5 + 0.5¥

Values are the mean ± SEM; n indicates the sample size. bpm, beats per minute; EDV, end-diastolic volume; ESV, end-systolic volume; GCS, global circumferential strain; IVS, interventricular septum, PWT; infarcted wall thickness; S, systole; d, diastole mm, millimeter; μl, microliter; ¥p< 0.05, vs. day 0 naïve control (No-MI).

Figure 1.

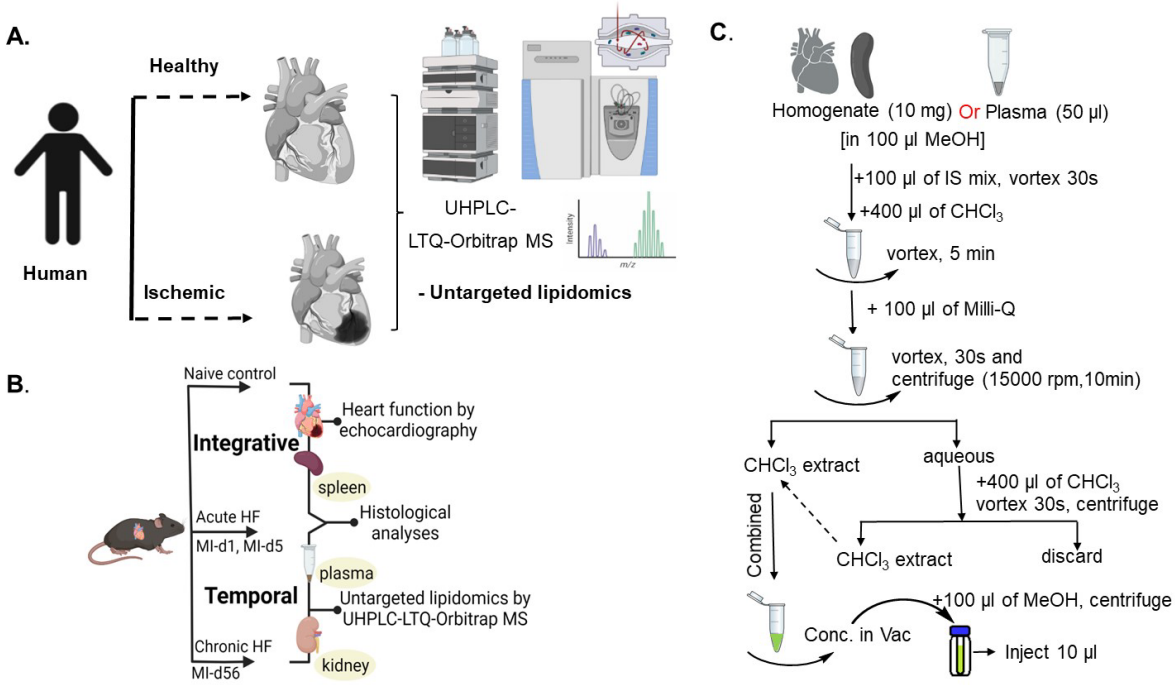

Figure 1. Experimental design and workflow of lipid extraction. **A.** Clinical sample analysis of healthy and ischemic patients. **B**. Temporal study design strategy in the rodent HF model. **C.** Procedure flowchart of total lipid extraction for MS/MS analyses. Partially created with Bio Render; published with permission

Figure 2.

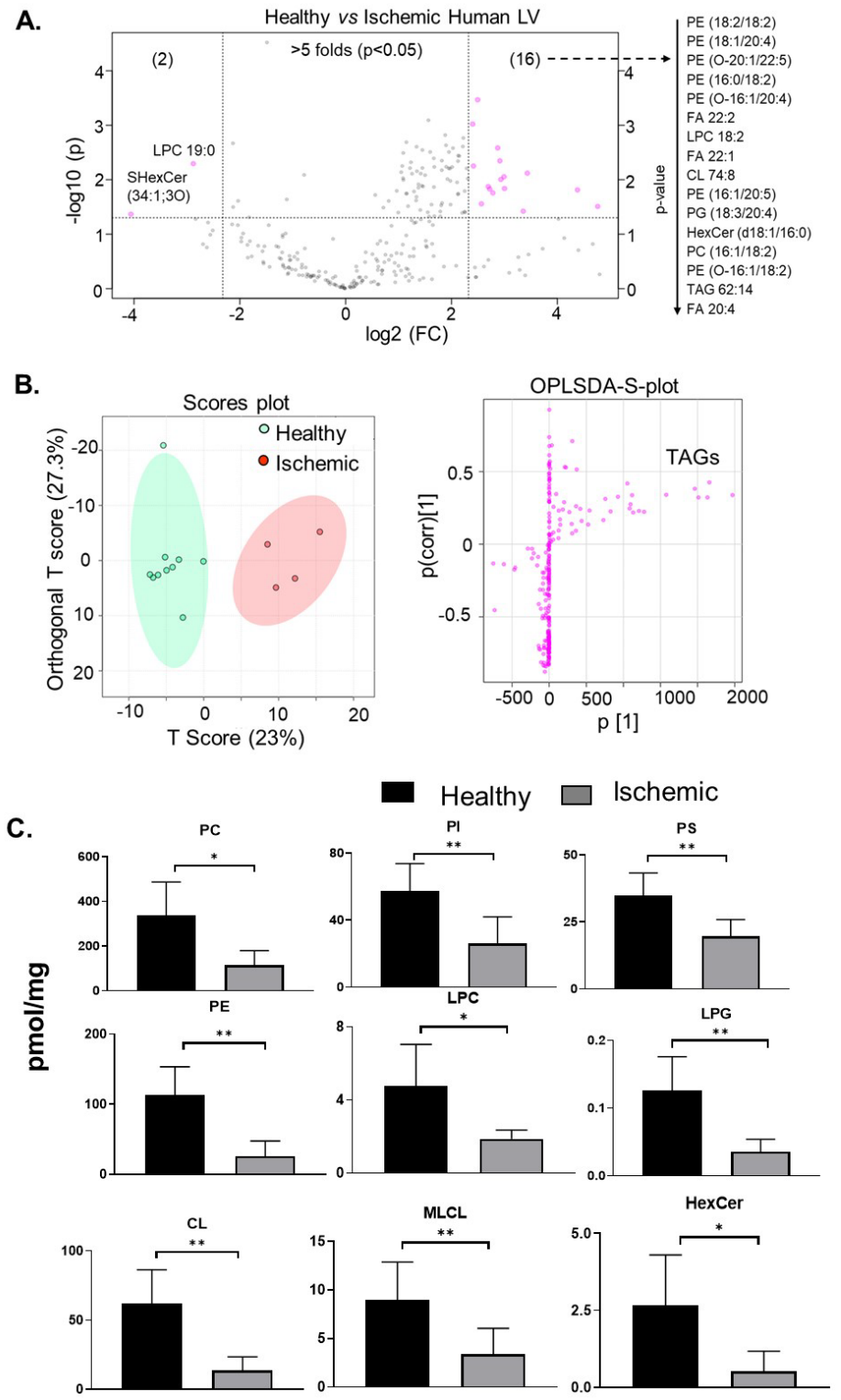

Figure 2. Altered lipid signatures in the human failing heart (healthy (n=10), ischemic (n=4)). **A.** Volcanic plot representing significantly altered lipids (t-test, $p<0.05$). B. Orthogonal projections of latent structures discriminant analysis (OPLSDA) and S-Plot

graphs demonstrating effects of ischemic LV on lipidomic profiles (model cross-validation results: R2X (p1= 0.23, o1=0.27), R2Y (p1=0.70, o1=0.11), Q2 (p1=0.41, o1=0.02), R2X, R2Y represents the model interpretation rate; Q2 indicates the model predictive ability; R2Y and Q2 closer to 1 indicates that the model is more reliable. Green spots represent samples from healthy human heart, while the red pots represent samples from ischemic patient LV. **C.** Bar charts representing significantly altered lipid classes (unpaired t-test, ****p<0.0001, ***p<0.0002, **p<0.0021, *p<0.0332).

Figure 3.

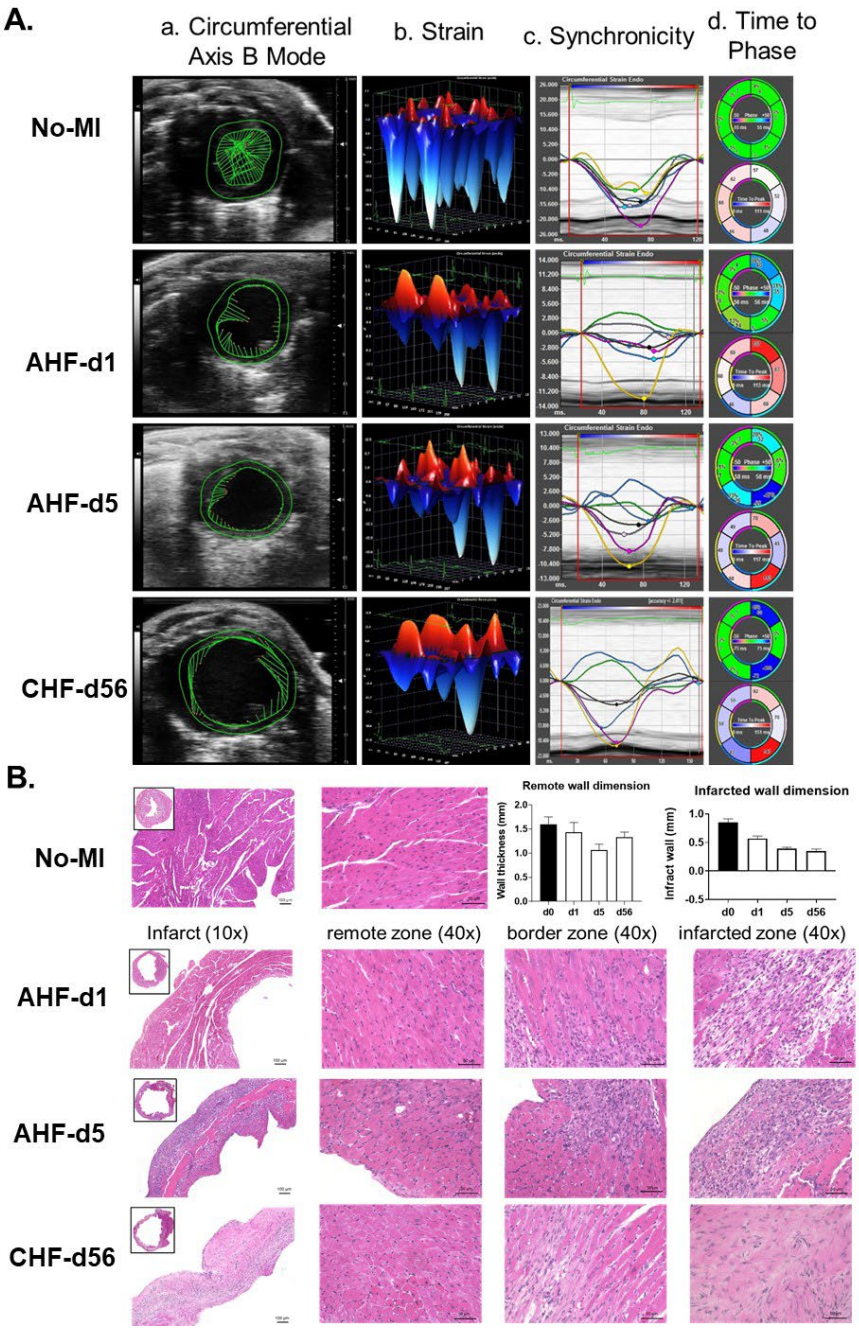

Figure 3. Temporal kinetics of functional and structural changes in acute and chronic heart failure in mice. **A:** Representative echocardiographic traces of temporal kinetics of short-axis B-mode circumferential strain (two-dimensional, 2-D and three-dimensional, 3-D) and segmental strain indicative of progressive, dynamic changes in left ventricle (LV) size, shape, and function in acute heart failure (AHF) and chronic heart failure (CHF) after myocardial infarction (MI). a: speckle-tracking based analysis using short-axis B-mode; the LV ultrasound image is presented in mid-systole. b and c: circumferential three-dimensional strain and segmental synchronicity of the LV. d. Time of phase after MI in progressive HF. Images are representatives of n = 6–9 mice/group/time day point. **B**: time-dependent structural changes in the infarct, peri-infarct (border zone), and remote (non-infarcted) areas in AHF and CHF pathophysiology of LV post-MI. Hematoxylin and eosin (H&E) staining of X1.25, (a) images of the left ventricle (LV) mid-cavity insert with 10x suggestive wall-thinning with HF progression , X40 (b) images of the remote zone, X40 (c) images of the peri-infarct/border zone, and X40 (d) images of the infarct zone in C57BL/6 mice during AHF and CHF post-MI displaying changes in myocardium ultrastructure, n = 4–6 mice/group/day time point. Scale bar = 50 μm.

Figure 4.

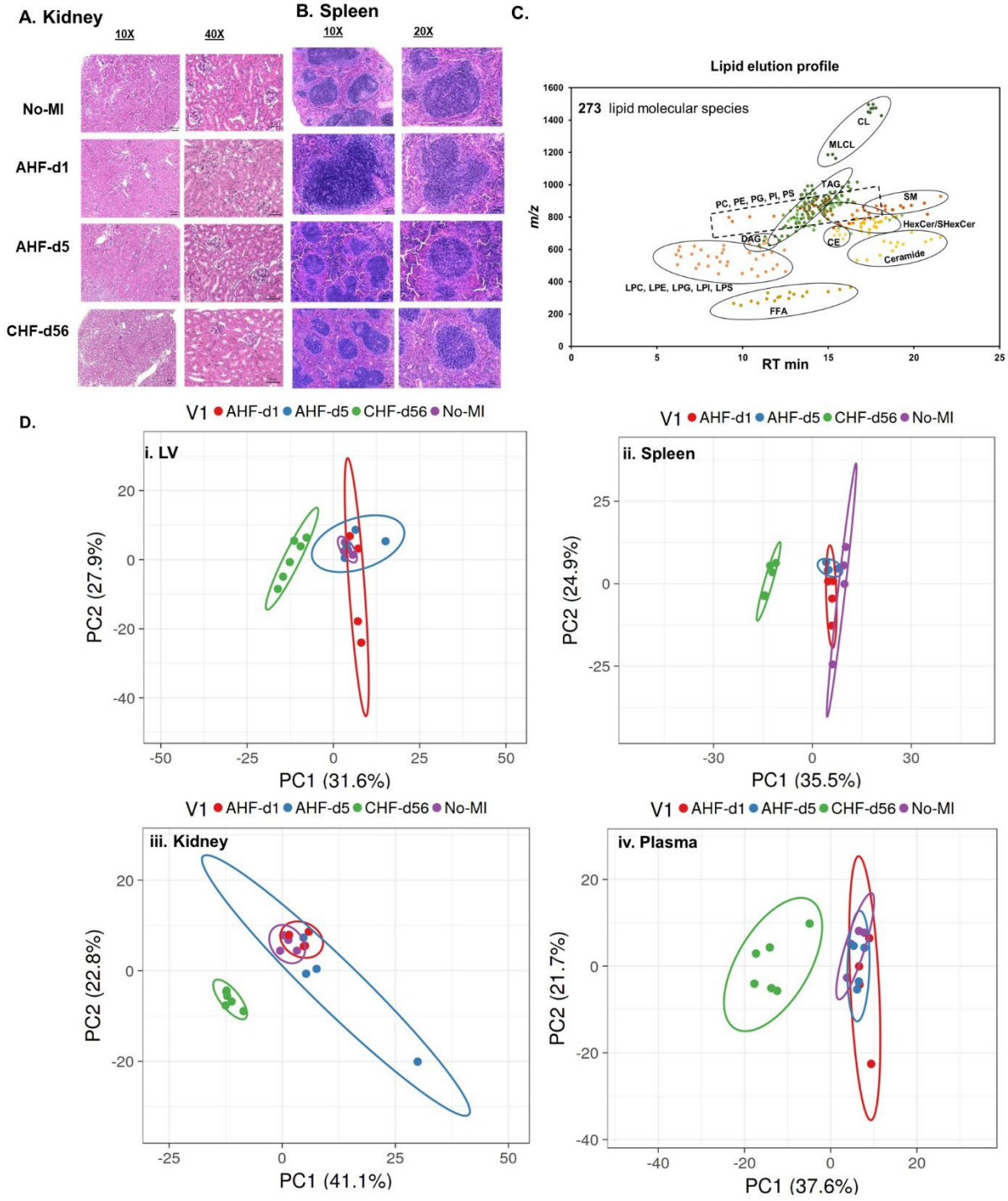

Figure 4. Kidney and spleen histology and multivariate analysis of total lipids in the progessionfrom acute to chronic HF. Representative X10 and X40 H&E-stained kidney (**A**) and spleen (**B**) images from controls (No-MI), MI-d11 (AHF), MI-d5 (AHF), and MI-d56 (CHF), n = 4–6 mice/group. Scale bar = 100 μm. **C.** Lipid classes detected and their elution profile. **D.** Principal component analysis (PCA) score plots of total lipids in the LV (i), spleen (ii), kidney (iii), and plasma (iv).

Figure 5.

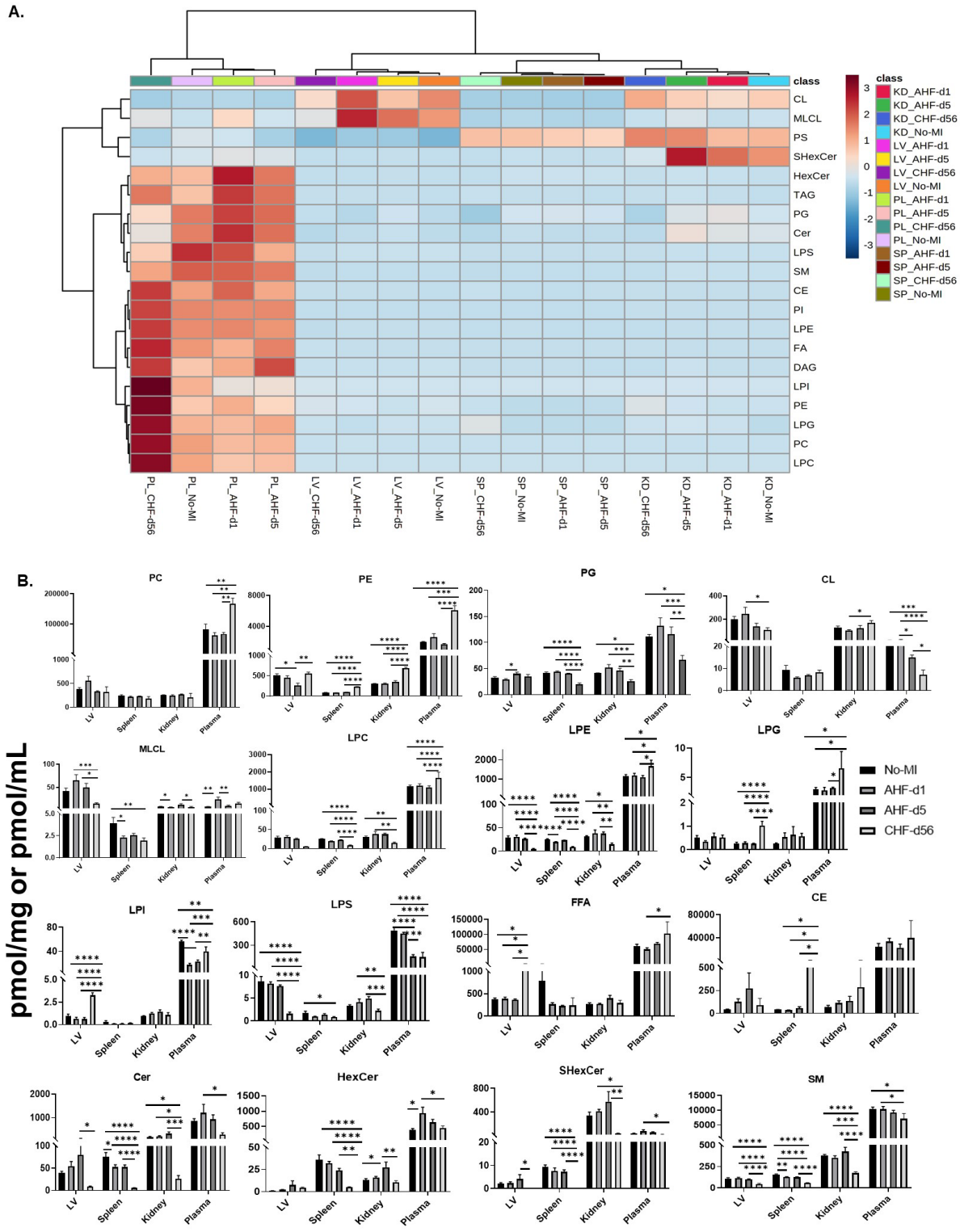

Figure 5. Relative levels of class-specific lipidomic changes and their hierarchical cluster correlation analysis. **A**. Heatmap representing the variance in lipid levels (distance measure: Euclidean, clustering method: ward, with variance (ANOVA) (PL: Plasma, KD: Kidney, LV: Left ventricle, SP: spleen). **B**. Bar graphs representing class-specific changes in lipid profiles (Ordinary one-way ANOVA was applied and the

significance levels were decided as follows: with GP (GraphPad) value of 0.1234 (ns), 0.0332 (*), 0.0021 (**), 0.0002(***), 0.0001(****).

Figure 6.

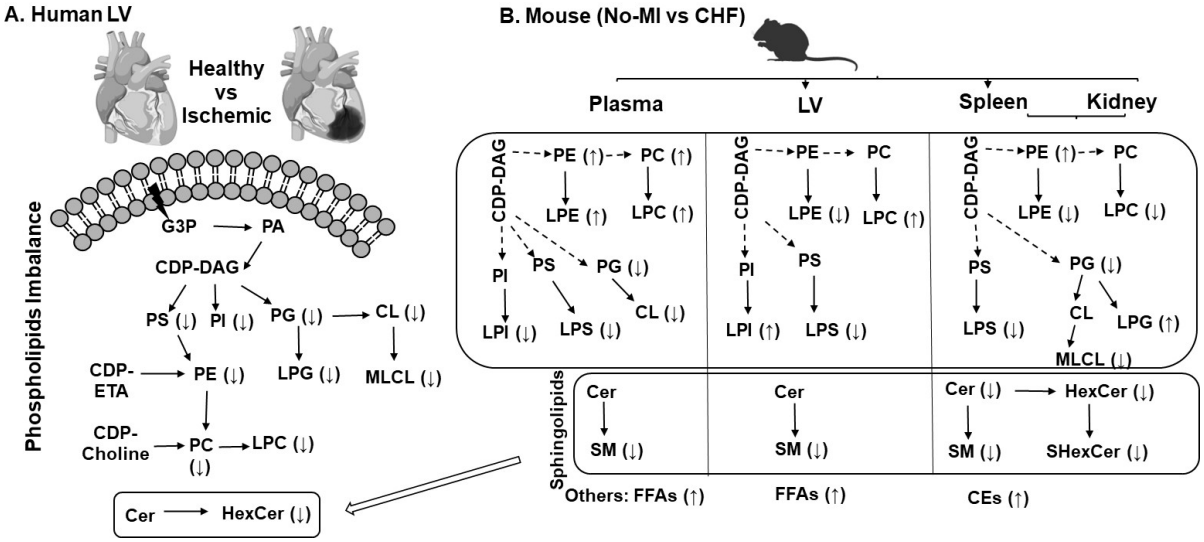

Figure 6. Summarized pathway of lipidomic changes in human failing heart and mice with CHF. The lipid classes are depicted based on their biosynthesis. (↓) indicates the downregulation of the lipid class and (↑) indicates the upregulation of the lipid class between control vs ischemic LV in human and No-MI vs CHF in mice plasma and organs.